frontiers | Frontiers in Marine Science

TYPE Original Research
PUBLISHED 01 March 2023
DOI 10.3389/fmars.2023.1139591

Check for updates

OPEN ACCESS

EDITED BY
Ya Ping Wang,
East China Normal University, China

REVIEWED BY
Weizeng Shao,
Shanghai Ocean University, China
Xiaoyun Li,
Shaanxi Normal University, China
Bin Liu,
Lynker Technologies LLC, United States
Zhixiang Jiang,
Qingdao University, China

*CORRESPONDENCE
Jing Yu
by6801@ouc.edu.cn
Hao Zheng
zhenghao2013@ouc.edu.cn

†These authors share first authorship

SPECIALTY SECTION
This article was submitted to Coastal Ocean Processes, a section of the journal Frontiers in Marine Science

RECEIVED 07 January 2023
ACCEPTED 14 February 2023
PUBLISHED 01 March 2023

CITATION
Sun H, Zheng K, Yu J and Zheng H (2023) Spatiotemporal distributions of air-sea CO_2 flux modulated by windseas in the Southern Indian Ocean. *Front. Mar. Sci.* 10:1139591. doi: 10.3389/fmars.2023.1139591

Spatiotemporal distributions of air-sea CO_2 flux modulated by windseas in the Southern Indian Ocean

Huiying Sun[1†], Kaiwen Zheng[2†], Jing Yu[1,3*] and Hao Zheng[4,5*]

[1]College of Oceanic and Atmospheric Sciences, Ocean University of China, Qingdao, China, [2]Frontier Science Center for Deep Ocean Multispheres and Earth System (FDOMES), Physical Oceanography Laboratory, Ocean University of China, Qingdao, China, [3]Institute of Marine Development of Ocean University of China, Qingdao, China, [4]Key Laboratory of Marine Environment and Ecology, Institute of Coastal Environmental Pollution Control, College of Environmental Science and Engineering, Ministry of Education, Frontiers Science Center for Deep Ocean Multispheres and Earth System, Ocean University of China, Qingdao, China, [5]Sanya Oceanographic Institution, Ocean University of China, Sanya, China

The Southern Indian Ocean is a major reservoir for rapid carbon exchange with the atmosphere, plays a key role in the world's carbon cycle. To understand the importance of anthropogenic CO_2 uptake in the Southern Indian Ocean, a variety of methods have been used to quantify the magnitude of the CO_2 flux between air and sea. The basic approach is based on the bulk formula—the air-sea CO_2 flux is commonly calculated by the difference in the CO_2 partial pressure between the ocean and the atmosphere, the gas transfer velocity, the surface wind speed, and the CO_2 solubility in seawater. However, relying solely on wind speed to measure the gas transfer velocity at the sea surface increases the uncertainty of CO_2 flux estimation. Recent studies have shown that the generation and breaking of ocean waves also significantly affect the gas transfer process at the air-sea interface. In this study, we highlight the impact of windseas on the process of air-sea CO_2 exchange and address its important role in CO_2 uptake in the Southern Indian Ocean. We run the WAVEWATCH III model to simulate surface waves in this region over the period from January 1st 2002 to December 31st 2021. Then, we use the spectral partitioning method to isolate windseas and swells from total wave fields. Finally, we calculate the CO_2 flux based on the new semiempirical equation for gas transfer velocity considering only windseas. We found that after considering windseas' impact, the seasonal mean zonal flux (mmol/m^2·d) increased approximately 10%-20% compared with that calculated solely on wind speed in all seasons. Evolution of air-sea net carbon flux (PgC) increased around 5.87%-32.12% in the latest 5 years with the most significant seasonal improvement appeared in summer. Long-term trend analysis also indicated that the CO_2 absorption capacity of the whole Southern Indian Ocean gradually increased during the past 20 years. These findings extend the understanding of the roles of the Southern Indian Ocean in the global carbon cycle and are useful for making management policies associated with marine environmental protection and global climatic change mitigation.

KEYWORDS

greenhouse gases, gas transfer velocity, surface wave breaking, air-sea CO_2 flux, Southern Indian Ocean

1 Introduction

Human activities have been a major source of global warming over the past 50 years (IPCC, 2022a). Anthropogenic emissions of greenhouse gases have persisted since 1990. By 2019, carbon dioxide (CO_2) from fossil fuels and industry had the largest growth in absolute emissions (IPCC, 2022b). Although CO_2 accounts for approximately 20% of greenhouse gases, it is responsible for 80% of the radiative forcing that sustains the greenhouse effect and makes the atmospheric temperature continuously rise (Lacis et al., 2010; Schmidt et al., 2010). Since the beginning of the industrial era, global anthropogenic CO_2 emissions from human activities such as the burning of fossil fuel, cement production, and changing land use have increased over time, and the present atmospheric carbon concentration has been unprecedented in the last three million years (Willeit et al., 2019). The accumulation of discharged atmospheric CO_2 rose from 277 ppm in 1750 to 414.4 ppm in 2021, well beyond the normal range of natural variability (Levitus et al., 2000; Feely et al., 2001; Joos and Spahni, 2008; Lekshmi et al., 2021). Therefore, the accurate evaluation of anthropogenic emissions and the world's carbon cycle has been of great scientific interest in recent years.

The ocean is an important active carbon reservoir, taking up more than 25%-30% of anthropogenic CO_2 emitted to the atmosphere; so it plays a pivotal role in mitigating global climate change (Sabine et al., 2004; Friedlingstein et al., 2020). The Southern Indian Ocean, spanning from 0° to 66.5°S, is one of the largest oceanic sinks of anthropogenic CO_2, representing approximately 10% of the ocean surface area but removing 15% of CO_2 emitted by humans (Frölicher et al., 2015; Gruber et al., 2019). The Southern Indian Ocean is unique because of its geographical features, atmospheric forcing, and complex ocean dynamics. In contrast to the Pacific and the Atlantic, it is completely enclosed by the Indian subcontinent in the north and is dominated by westerlies near the equator rather than trade winds (Valsala et al., 2012). Annual wind speeds in this region are higher than those of other seas at the same latitudes, which increases the gas transfer velocity and thus accelerates the CO_2 exchange between the sea surface and atmosphere (Deacon, 1977; Wanninkhof, 2014; Watson et al., 2020).

To understand the importance of anthropogenic CO_2 uptake in the Southern Indian Ocean, a variety of methods have been used to quantify the magnitude of the CO_2 flux between the sea and air (Metzl et al., 1995; Louanchi et al., 1996). Typical approach based on the bulk formula—the air-sea CO_2 flux is commonly calculated by the difference in CO_2 partial pressure between the ocean and the air (pCO_2^{sea} and pCO_2^{air} , respectively), the gas transfer velocity, contemporaneous sea surface wind speed, and the CO_2 solubility in seawater (Takahashi et al., 2002; Sabine et al., 2004; DeVries, 2014; Frölicher et al., 2015; Roobaert et al., 2019). Using this approach, a series of crucial results have been reported in the last 20 years (e.g., Bates et al., 2006; Wanninkhof and Triñanes, 2017; Vieira et al. 2020). However, relying solely on wind speed to calculate the gas transfer velocity at the sea surface increases the uncertainty of CO_2 flux estimation (Woolf, 1993). Recent studies have shown that the generation and breaking of ocean waves also significantly affect the gas exchange process at the sea-air interface (Zappa et al., 2007; Gu et al., 2021). Observations in the Southern Indian Ocean sector of the Antarctic Circumpolar Current (ACC) show that large quantities of bubbles produced by wave breaking enhance the intensity of under-surface turbulence by up to three orders of magnitude and hence expand the gas contact area (Li et al., 2021). This will substantially increase gas transfer velocity and thus enhance CO_2 absorption by the ocean. To address the important role of surface wave breaking on CO_2 exchange, a new semiempirical equation for gas transfer velocity has recently been proposed that can account for different significant wave height (SWH hereafter) and divide gas transfer velocity into turbulence and bubbles contributions. Calculations after this upgrade significantly reduce the uncertainty of gas transfer velocity at moderate-high wind speeds (Deike and Melville, 2018). And the contribution of bubbles and the dependence of the ocean state vary greatly on regional and seasonal scales, generally supporting the ocean to absorb approximately 40% of the CO_2 (Reichl and Deike, 2020). Gu et al. (2021) investigated a new expression of gas transfer velocity that coupled with wind-wave and showed that about 50% of the global CO_2 fluxes at high wind speeds are attributable to bubble-mediated contributions. However in these studies, 'wind-wave' represents total waves and using these to modulate gas transfer velocity may exaggerate their impacts.

Surface waves consist of swells and windseas, which are two categories with completely different characteristic features (Wang and Huang, 2004). Swells usually have regular shapes, more orderly arrangements with longer crest lines and smooth surfaces. They are stable as due to the action of air resistance and the internal friction of sea water, the wave energy is distributed in a larger area, and the energy and wave height of a swell in the water column decrease continuously during propagation (Zhang et al., 2011; Ethamony et al., 2013). As the period increases, the wavelength and wave speed grow correspondingly, which makes the steepness of the wave surface decrease. Hence swells will not produce large numbers of bubbles in the sea-air interface. In contrast to swells, windseas are locally generated, have short wavelengths, are more chaotic, and travel more slowly than surface wind. Windseas gain energy from wind to grow and easily lose instability and break, which significantly affects the gas exchange process in the sea-air interface (Qian et al., 2020). Now that total waves include two categories, using total waves to quantify the gas transfer velocity might overestimate the impact of waves on the overall CO_2 flux.

Therefore, in this study, we highlight the influence of windseas on air-sea CO_2 exchange process and address the important role of surface waves in CO_2 absorption in the Southern Indian Ocean. We run the WAVEWATCH III model to simulate surface waves in the Southern Indian Ocean over the period from January 1st 2002 to December 31st 2021. Then, we use the spectral partitioning method to isolate windseas and swells from total wave fields. Finally, we calculate CO_2 flux based on the new semiempirical equation for gas transfer velocity considering only windseas. The article is structured as follows. Section 2 discusses the model configuration of the simulations and the data source we used to validate the model output. Spectral partitioning method to separate windseas and swells are discussed. We also present the standard bulk formula of air-sea CO_2 exchange flux and bulk formula modulated by windseas in this section. Section 3 first shows the simulated results of the spatial and seasonal distributions of the SWH of windseas and swells in the Southern Indian Ocean. Then, the validation results of the model output and observation data are discussed. Finally, the temporal and spatial distributions of air-sea CO_2 exchange flux modulated by windseas, differences between the calculations with/without waves' impact, and decadal trends of net carbon flux are presented. The overall implication and limitations of the study are evaluated in Section 4.

2 Data and methods

2.1 Configuration of wave simulations

We use the recent WAVEWATCH III (WW3, hereafter) official version 4.18 to simulate surface waves in the Southern Indian Ocean, spanning from 0° to 66.5°S. The specific settings are as follows: The wind speed—the 10 m wind above the surface—obtained from the European Centre for Medium-Range Weather Forecasts (ECMWF) ERA-5 datasets over the period from January 1st 2002 to December 31st 2021. The wind fields are regularly gridded and from 0° to 66.5°S, 30°E to 135°E with a 1/4° resolution. The time resolution is set to 6 hours. The water depth is automatically generated by the Gridgen 3.0 topography packet, which combines the National Geophysical Data Center - ETOPO 1 data. The topography resolution is 1/20°. Our model integrates the spectrum to a cut-off frequency f_{HF} and uses a parametric tail to frequency above f_{HF}. Twenty-four discrete wavenumbers (0.0412~0.4060Hz, 2.4~24.7s) and 36 directions are used to simulate isotropic waves. Parameterizations for current waves, wave-wave interactions, wave breaking-related white capping, wave refraction and shoaling are added to further improve the accuracy of the simulated waves (Hanson et al., 2006). Field model results, including 10-m wind speed, SWH of total waves, and wave energy density spectra, are output at each grid point with a time interval of 6 hours. We also output 4 points' wave information according to the position shown in Figure 1, which will be used for model validation against altimeters in the following section 2.2. Although ERA-5 datasets also provide wave reanalysis data that contain partition results of swells and windseas, significant numerical and physical differences can still be found between the WW3 and WAM models (Liu et al., 2002).

2.2 Modelling validation

In this study, we use altimeter data to evaluate our model performance. Data are obtained from the Australian Integrated Marine Observing System (IMOS), CRYOSAT-2 altimeter database. This data source provides global wave observations from altimeter products that have been put to use since 1985. All the wave heights have been verified against global float/buoy data at all crossover points with independent missions. Calibration details can be found in Ribal and Young (2019). In this study, we randomly selected four positions (shown in Figure 1) over a period from January 1st 2002 to December 31st 2021, for model validation. The SWH of total waves simulated by the WW3 model were compared to the altimeter data through temporal correlation analyses. We also calculated the bias and correlation coefficient between the model output and altimeter data to quantify the comparison results. All results are shown in Figure 2. The SWH produced by the model shows a clear temporal correlation with real-time data altimeter

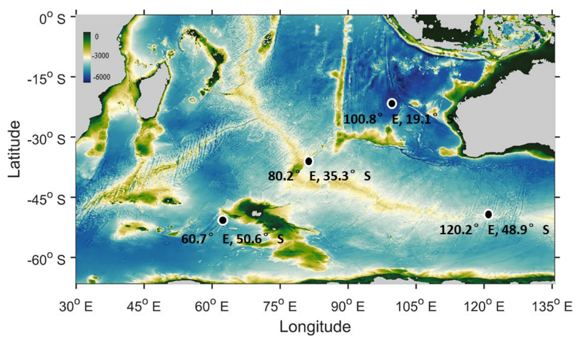

FIGURE 1
A map of the study region showing water depth in the Southern Indian Ocean, with the altimeter locations used for model verification. Four positions (60.7°E 50.6°S; 80.3°E 35.3°S; 100.8°E 19.1°S; 120.2°E 48.9°S) are randomly picked over a period from January 1st 2021 to December 31st 2021.

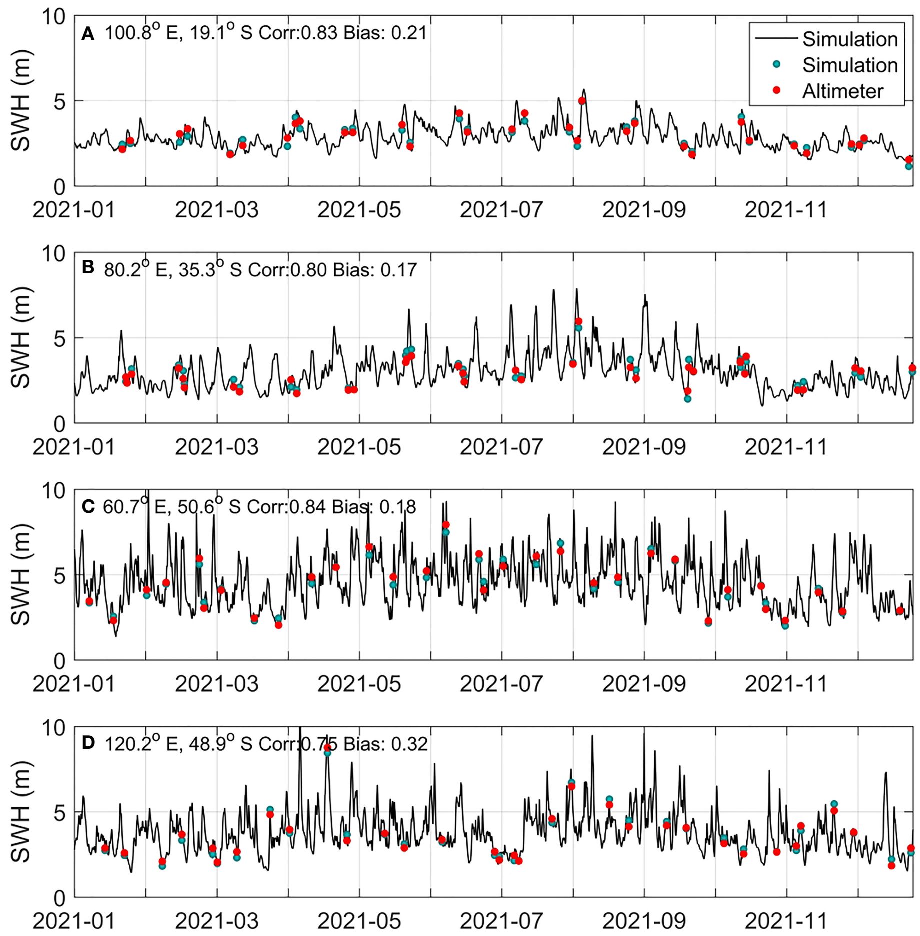

FIGURE 2
Time series of SWH comparisons between model outputs and altimeter records. Scatter points are results of model (green) and altimeter (red) correspond to a same moment. **(A–D)** are four panels of the four randomly selected locations.

observations. The correlation indexes are over 0.75-0.84, and the biases are less than 0.17-0.32 in all four positions, indicating that our model basically reflects the main wave information in the Southern Indian Ocean.

2.3 The spectra energy partition method

The version of WW3 used in this study contains a partition module that can separate swells and windseas from total waves. The partition module was at first used as the topography processing watershed algorithm by Hanson and Jensen (2004) to isolate a 2D wave spectra. Then, modified FORTRAN routines (Hanson et al., 2006) were added into the WW3 model to identified different waves. The basic principle is inverting 2D wave spectra and making spectral peaks become catchments. Then partition boundaries or watershed lines can be identified using the watershed algorithm. Swells and windseas are determined using wave age criterion on the basis of different components of wind direction and absolute speed. This method has proven to be highly accurate and were added into the WW3 model to identified different waves (Zheng et al., 2016; Tao et al., 2017; Anoop et al., 2020).

2.4 Calculation of air-sea gas exchange flux with no waves

We calculated the air-sea gas exchange flux of CO_2 (F,mol/m^2·d) with no waves using a standard bulk formula by Wanninkhof (2014):

$$F = k_0 L \Delta pCO_2 \tag{1}$$

where positive values of Fdenote the transfer of CO_2 from the ocean towards the atmosphere, negative values correspond to that from the atmosphere into the ocean, and L (mol(kg·atm)$^{-1}$) is the solubility of CO_2 in water (Weiss, 1974):

$$lnL = Al + A2100SST + A3ln100SST + SSSB1 + B2SST100 + B3SST1002 \tag{2}$$

Here, we used A_1 = -60.2409, A_2 = -93.4517, A_3 = 23.3585, B_1 = 0.023517, B_2 = -0.023656, and B_3 = 0.0047036. In addition, SST is the sea surface temperature in degrees Celsius and SSS is the sea surface salinity. k_0 is the appropriate gas transfer velocity calculated as $k_0 = 0.251 \quad U_{10}^2(Sc/660)^{-0.5}$, where U_{10} is the wind speed measured 10 m above the sea surface. The constant value of 0.251 is based on an extensive collection of gas transfer velocity estimates from Wanninkhof (2014). The variable Sc is the Schmidt number:

$$Sc = a + b(SST) + c(SST)^2 + d(SST)^3 \tag{3}$$

where a = 2073.1,b =125.62, c = 3.6276, and d = 0.043219 are all constant values applied from parameterization by Wanninkhof (2014). $\Delta pCO_2(pCO_2^{sea} - pCO_2^{air})$ is the CO_2 partial pressure difference between the surface seawater and the air.

We calculated F for each 1/4° × 1/4° latitude-longitude grid point in the open water of the Southern Indian Ocean over the period 2002 to 2021. For variables, the following data products were used. Monthly mean SSTs were employed from the Advanced Microwave Scanning Radiometer (AMSR) datasets with two satellites provided by the Romete Sensing System, namely, AMSR-2 and AMSR-E. U_{10} is an ERA-5 dataset of ECMWF from 1979 to the present. Monthly mean SSS is available at the Physical Sciences Laboratory (PSL) of the National Oceanic and Atmospheric Administration (NOAA). SSS is a product of the NCEP Global Ocean Data Assimilation System, which is forced by the momentum flux, heat flux, and fresh water flux from the NCEP atmospheric reanalysis (GODAS, Behringer et al., 1998). It reproduces observations well and is now the most commonly used dataset for F analysis (e.g., Watson et al., 2020; Monteiro et al., 2020; Zheng et al., 2021). For the ΔpCO_2, we employed the observation-based global monthly gridded atmospheric and sea surface CO_2 partial pressure and CO_2 fluxes product by Landschützer et al. (2020) from 1982 onwards. These observation-based data were obtained using a two-step artificial neural network method combining biogeochemical provinces and CO_2 driver variables and observations from the fourth release of the Surface Ocean CO_2 Atlas (SOCAT, Bakker et al., 2016).

2.5 Calculation of air-sea gas exchange flux with waves

To stress the important role of ocean surface waves in air-sea CO_2 exchange, we used a wind-wave-dependent expression by Deike and Melville (2018) to estimate the CO_2 exchange rate, k_w. k_w consists of two terms, bubble-mediated k_{wb} and nonbubble k_{wnb}, given as:

$$k_w = k_{wb} + k_{wnb}$$
$$= \frac{A_B}{L \cdot R \cdot SST} u_*^{5/3}(gH_s)^{2/3}\left(\frac{Sc}{660}\right)^{-1/2} + A_{NB}u_*\left(\frac{Sc}{600}\right)^{-1/2} \tag{4}$$

where $A_B = 1 \pm 0.2 \times 10^{-5} s^2 m^{-2}$ is a dimensional fitting coefficient, $A_{NB} = 1.55 \times 10^{-4}$, $R = 0.08205\ L\ atm\ mol^{-1} k^{-1}$is the ideal gas constant (Keeling, 1993), g is the gravitational acceleration, and H_s is the SWH from the WW3 model simulated waves. $u_* = (\tau/\rho_{air})^{1/2}$ is the friction velocity in the air, where ρ_{air} is the mean air density and τ is a turbulent shear stress. Then, the calculated k_w is substituted into equation (1) to further calculate the F under the impact of waves. The data sources used in this study are listed in Table 1.

3 Results

3.1 Separation of swells and windseas from total waves in the Southern Indian Ocean

Seasonal distributions of SWH (including total waves, windseas, and swells) are showed in Figure 3. The highest seasonal mean SWH of total waves, windseas and swells are found in the extratropical

TABLE 1 Descriptions of data used in this study and their sources.

Name	Datasets	Resolution	Coverage time	Source	Download link
U_{10}	ERA-5	1/4°	1979-present	European Centre for Medium-Range Weather Forecasts	https://www.ecmwf.int/en/forecasts/datasets/reanalysis-datasets/era5
SWH	CRYOSAT-2	1°	2010-present	Australian Ocean Data Network	https://thredds.aodn.org.au/thredds/catalogue/IMOS/SRS/Surface-Waves/Wave-Wind-Altimetry-DM00/CRYOSAT-2/catalogue.html
Water depth	ETOPO1	1/60°	—	National Geophysical Data Center	https://www.ngdc.noaa.gov/mgg/global/
SST	AMSR	1/4°	2002-present	NASA AMSR-E Science Team and NASA Earth Science MEaSUREs Program	https://www.remss.com/missions/amsr
SSS	NCEP-GODAS	0.333°x1.0°	1980-present	NOAA Physical Sciences Laboratory	https://psl.noaa.gov/data/gridded/data.godas.html
$pCO_2^{sea} \cdot pCO_2^{air}$	Global monthly gridded sea surface pCO_2 product	1°	1985-present	NOAA National Centers for Environmental Information	https://www.ncei.noaa.gov/data/oceans/ncei/ocads/data/0160558/

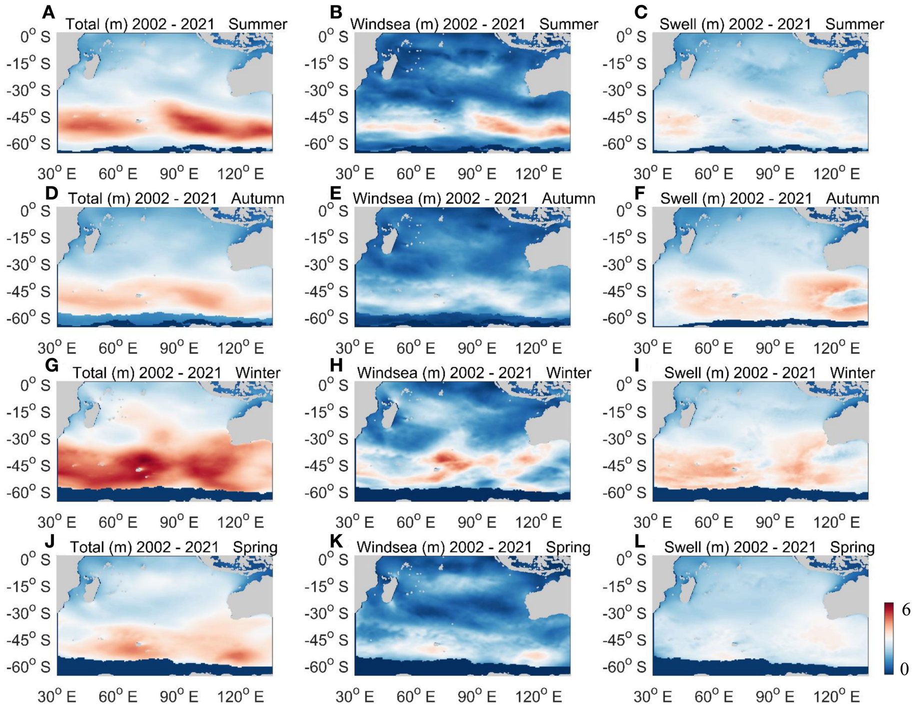

FIGURE 3
Seasonal averages for total SWH **(A, D, G, J)**, wave height of windseas **(B, E, H, K)**, and wave height of swells **(C, F, I, L)** in the Southern Indian Ocean.

areas, which are basically distributed along the southern westerlies. SWH also shows obviously seasonal variations in the whole Southern Indian Ocean. The strongest wave energy appears in summer, followed by winter. The wave heights depend greatly on the seasonal changes in wind speed; windseas are clearly aligned with the winds, as powerful westerly winds directly generate strong windseas (Semedo et al., 2011). The westerly region in the Southern Indian Ocean are the main source areas of swells (Vincent and Soille, 1991) also make swells energy particularly high than low-latitude region. Apart from these seasonal and spatial results that are consistent with previous surface wave studies (Zheng et al., 2016), our partition results provide an interesting view: windseas contribute only a small fraction of energy to the total waves in almost every region and season. In high- and middle-latitude areas (30°S-60°S), the windseas energy in winter accounts for the largest proportion, 37.26%, followed by summer, which is 25.09%. In low- and middle-latitude areas (0-30°S), summer and winter also have a higher windseas proportion but maintain less than 40% of total waves. As we discussed above, windseas have completely different physical properties with swells and should be the main factor

TABLE 2 The regional partition distribution of windseas energy to total waves in different seasons.

Seasons	0-30°S	30-60°S
Spring	6.43%	9.53%
Summer	37.26%	35.71%
Autumn	15.09%	8.22%
Winter	25.09%	21.17

influencing gas transfer velocities (Jiang and Chen, 2013). We suggest that modifying the air-sea CO_2 exchange flux by using total waves tends to overestimate the effect of waves. The specific proportion of windseas energy to total waves is shown in Table 2. In the following sections, we emphasize the effect of windseas on the air-sea CO_2 exchange flux in the southern Indian Ocean.

3.2 Spatial and temporal characteristics of air-sea CO_2 flux modulated by windseas

We first showed an important but independent driver—surface seawater partial pressure (pCO_2^{sea})—that affects air-sea CO_2 transfer in the Southern Indian Ocean. Because the atmospheric partial pressure of CO_2 (pCO_2^{air}) is nearly consistent in the open ocean, pCO_2^{sea} largely determines the direction and rate of CO_2 transfer through the air-sea interface (Takahashi et al., 2002). Study has shown that the majority of the seasonal and spatial variations in CO_2 flux stem from the pCO_2^{sea} (McGillis et al., 2001). Therefore, here, before carefully discussing the distribution and variation of the air-sea CO_2 flux, we first examined the spatial distribution of the seasonal mean pCO_2^{sea} in the Southern Indian Ocean (Figure 4). The spatial pattern of pCO_2^{sea} showed an uneven distribution, and seasonal variation was also apparent. In autumn and winter, there was a large area of low pCO_2^{sea} in the wide sea area between 20°S and 40°S. In addition, as the area of the subtropical high-pressure belt increased with the onset of spring, a decrease in the low pCO_2^{sea} area occurred from south to north. A high pCO_2^{sea} zone emerged near 80° E and reached its maximum value of 380 μatm. In summer, the low pCO_2^{sea} region tended to be stable at approximately 40°S, and pCO_2^{sea}

10.3389/fmars.2023.1139591

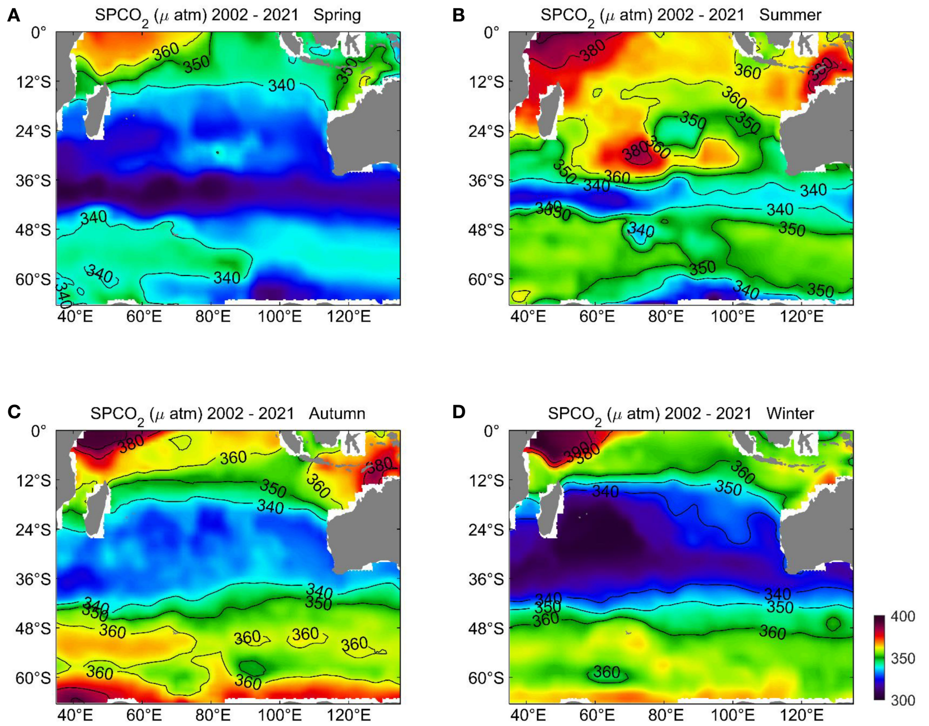

FIGURE 4
Seasonal distributions of surface seawater partial pressure of CO_2, pCO_2^{sea} (µatm), in the Southern Indian Ocean. **(A)** Spring, **(B)** Summer, **(C)** Autumn, **(D)** Winter.

followed by sea surface temperature variations. The pCO_2^{sea}in the Antarctic coastal waters was higher in autumn and winter, and lower in other seasons. Throughout the year, a high pCO_2^{sea} zone existed between 0°S and 12°S on the east coast of Africa, which was caused by the high-salinity and high-temperature water at the confluence of cold and warm currents in summer and the confluence of warm currents in winter (Deacon, 1981).

Surface wave breaking has an effect on gas transfer velocity. A higher gas transfer velocity will be generated for more developed windseas states under the same wind and pCO_2^{sea} (Zhao et al., 2003). To see this difference clearly, we show the temporal evolution of the gas transfer velocity with waves and no waves in Figure 5. Values at each point are annually averaged in the full region. It is clear that after considering the impact of windseas, the gas transfer velocity is improved nearly for all times. An average 5%-15% enhancement is seen, which is lower than the enhancement caused by total waves shown in Gu et al. (*2020*). This is in line with expectations, as increasing evidence has indicated that mass transfer, such as CO_2, is factually influenced by the surface turbulent process associated with the wave field (Liang et al., 2013*;* Brumer et al., 2017*;* Lenain and Melville, 2017). Surface wind is just an external forcing; as an indirect factor, it does not determine gas exchange (e.g., Edson et al., 2011*;* Liang et al., 2020). However, if windseas break, they generate large amounts of whitecaps, which will directly affect gas transfer through two mechanisms. First, breaking waves can promote the transfer associated with the upper turbulent patches. The interface contaminated by surface active impurities can be renewed by breaking waves, resulting in an accelerated increase in gas exchange in high wind speed areas (Komori and Misumi, 2002). Then there is a bubble-mediated transfer, in which the gas is trapped in a bubble for a certain period of time during the transfer between the air and the sea (Hasse and Liss, 1980*)*.

Based on the new gas transfer velocity, we then provide the distributions of seasonal mean CO_2 flux modulated by windseas in the Southern Indian Ocean in Figure 6. The distribution of CO_2 flux in the Southern Indian Ocean exhibited distinct regional and seasonal differences. The tropical area (0°-12°S) tended to lose a substantial amount of CO_2 through outgassing, mainly due to the high *SST* and low wind speeds throughout the year. Among them, the CO_2 uptake in summer was weak over the regions because of the uniform distribution of air pressure and the relative scarcity of low pressure systems in the atmosphere. Compared with the tropical area, the seasonal variation of CO_2 flux in the subtropical region (12°S-36°S) was more obvious. During the spring and winter, the

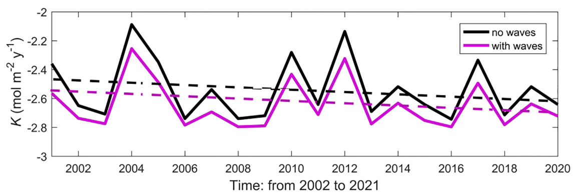

FIGURE 5
Temporal evolution of gas transfer velocity with waves (solid black) and no waves (solid purple).

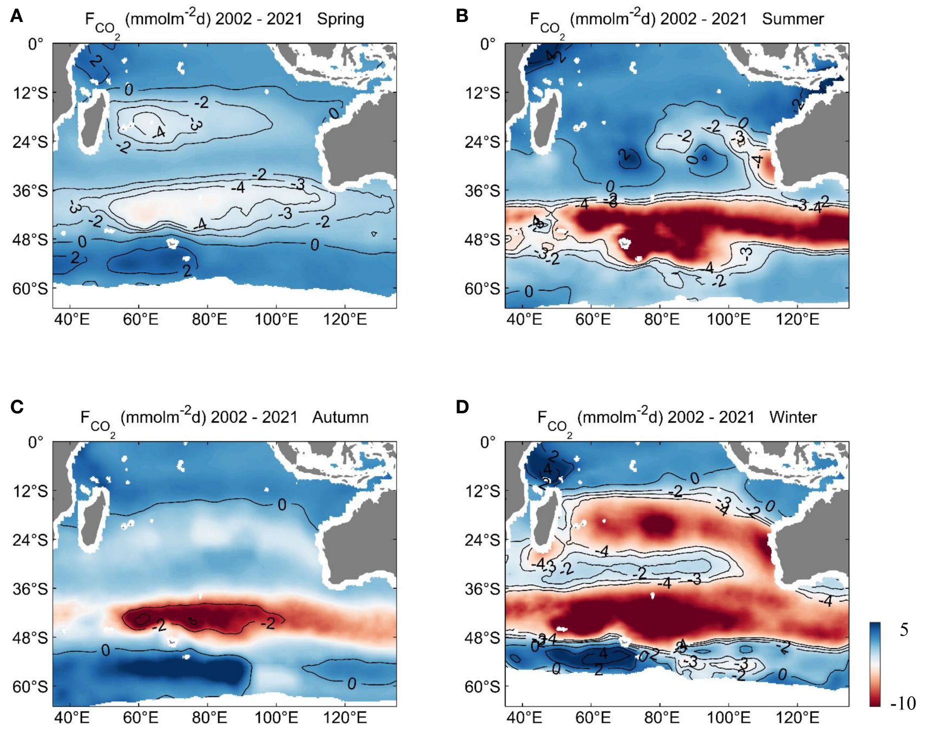

FIGURE 6
Seasonal distributions of air-sea CO_2 flux, *F* (mmol/m^2·d), in the Southern Indian Ocean. **(A)** Spring, **(B)** Summer, **(C)** Autumn, **(D)** Winter.

ability to absorb atmospheric CO_2 tended toward to be stronger than other seasons. In winter, controlled by the surface waves in the southeasterly trade winds, the CO_2 flux varied markedly. Strong trade winds in winter produced stronger wave fields leading to higher CO_2 flux, with an average maximum of -3.14 mmol/m^2·d in the central region between 12°S and 24°S. In the ACC region (36°S-52°S), the Southern Indian Ocean was a very strong sink of atmospheric CO_2 throughout the year, with the maximum mean uptake reaching -8.12 mmol/m^2·d. Strong westerly winds blowing across the sea give rise to abundant physical oceanographic processes, such as wind blocking, string, and high-pressure collapsing, may further strengthen the effect of windseas on the air- sea gas exchange (Toba and Koga, 1986; Toba, 1988). The majority of the net uptake occurred in winter, consistent with the findings of previous studies (Sarma et al., 2013; Zhang et al., 2017). Finally, similar to the tropical region, the entire subpolar region (52° S-62°S) tended to be a source of CO_2 to the atmosphere, because the horizontal temperature distribution was more uniform, the horizontal pressure gradient was very small, the air flow mainly converged and rose, the annual average wind speed is low which was unfavorable to the gas exchange process at the air-sea interface. Overall, annual mean value over the subpolar region is around -0.24 mmol/m^2·d. To clearly show the impact of windseas to the CO_2 flux, we show differences for the seasonal and spatial distributions between with and without windseas impact in Figure 7. Consistent with the regional distributions of partition results of windseas from total waves, the most significant differences appears in the southern westerlies areas. And for the seasonal aspect, the strongest CO_2 uptake increasement appears in summer and winter. The maximum increasement gets up to 20% which suggests that the windseas have considerable impact in the region. In contrast, low-latitude region and spring and autumn all have a relatively weak increasement response to the low energy of windseas there.

To further clarify the corresponding spatiotemporal relationships and reveal the long-term trend of air-sea CO_2 flux in the investigated two-decade time span, we show the zonal time series of air-sea CO_2 flux modulated by windseas for the entire Southern Indian Ocean in Figure 8. The overall pattern of CO_2 sources and sinks in the Southern Indian Ocean was relatively stable and had obvious temporal and spatial variations. In the tropical and subpolar regions, the Southern Indian Ocean was generally characterized by CO_2 sources with a weak interannual variation trend. The subtropical regions showed obvious seasonal variations, with sinks in winter and spring and sources in summer and autumn. The interannual variation remained unchanged in the 20-year time span included in this study. Obvious CO_2 source-to-sink and sink-to-source transition regions were found at approximately 25°S and 35°S, which was also consistent with observations (Jabaud-Jan et al., 2004; Xu et al., 2016; Lekshmi et al., 2021). The ACC region was a clear long-persisting CO_2 sink area, with increasing intensity of carbon absorption over time. We also found that approximately every seven years, a large CO_2 absorbing area formed, with effects covering 50 degrees of latitude from south to north. Each appearance of this area lasted for three years, and it contributed substantially to the net CO_2 uptake in the Southern Indian Ocean.

Figure 9 shows the 20-year zonal mean seasonal flux in the Southern Indian Ocean. To clearly highlight the impact of windseas on CO_2 exchange, we show the flux calculated from no

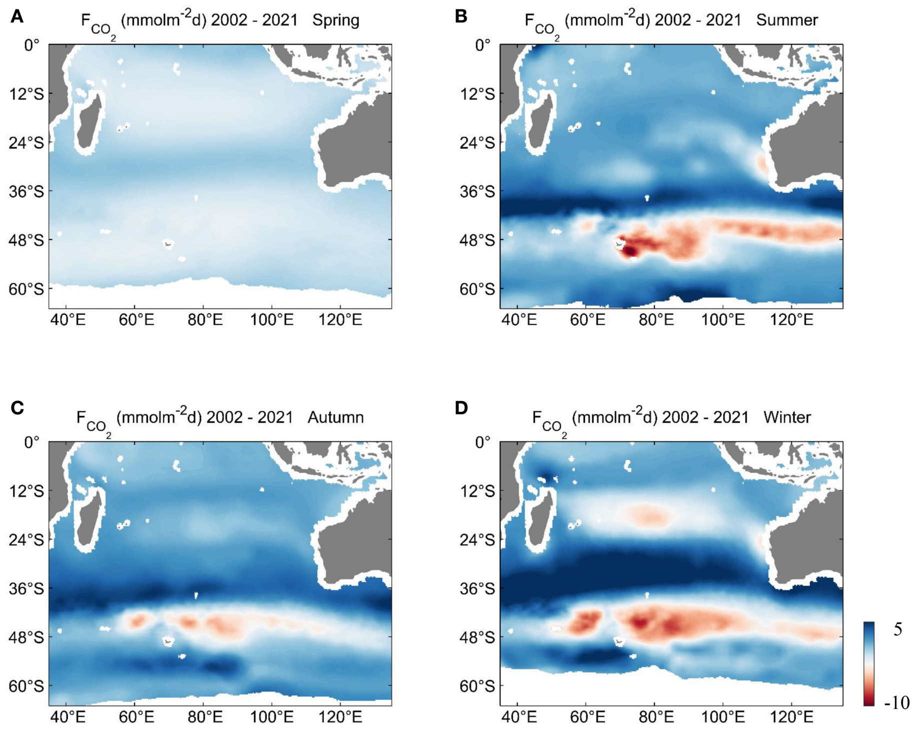

FIGURE 7
Differences for the seasonal and spatial distributions between with and without windseas impact. **(A)** Spring, **(B)** Summer, **(C)** Autumn, **(D)** Winter.

waves in dashed lines and with waves in solid lines in this figure. Both the calculations from the two methods show clear spatiotemporal characteristics. In terms of spatial distribution, the CO_2 flux was less than or near to zero between 12°S and 48°S, which means this region is a CO_2 sink or saturation area. The CO_2 flux of all seasons was generally greater than or equal to zero between 0°S and 12°S, indicating a moderate CO_2 source. In contrast, although the CO_2 flux fluctuated significantly with the seasons at south of 48°S, the total CO_2 emissions were stronger. The sea area near the Antarctic continent mainly presented a weak convergence source and saturation zone. In terms of the seasonal distribution of air-sea CO_2 flux, the most dramatic fluctuations with latitude occurred in winter. The CO_2 uptake of the Southern Indian Ocean repeatedly increased and decreased, showing a "W" pattern covering form approximately 12°S to 48°S, with more CO_2 absorption in the middle and high latitudes than in the lower latitudes; the peak values of CO_2 absorption in winter were -3.23 mmol/m^2·d with no waves and -3.31 mmol/m^2·d with waves, reached at 38°S and 40°S, respectively. In spring and autumn, there was weak CO_2 absorption at north of 30°S, whereas the south was a strong CO_2 sink area. The maxima of CO_2 absorption with the impact of windseas were -2.21 mmol/m^2·d and -4.48 mmol/m^2·d respectively, reached at approximately 45°S. Overall, the Southern Indian Ocean had the strongest CO_2 uptake in summer, with seasonal mean absorption of approximately -1.97 mmol/m^2·d under the influence of waves.

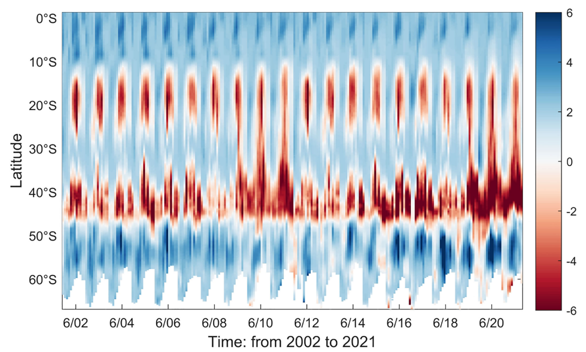

FIGURE 8
Zonal sequence diagram of *F* (mmol/m^2·d) from 2002 to 2021 in the Southern Indian Ocean.

3.3 Decadal CO_2 uptake trend predicted by the gas transfer velocity affected by windseas and no windseas

Finally, to further investigate the decadal CO_2 uptake trend and assess its important role in future carbon sequestration, we examined the seasonal evolution of air-sea net carbon flux (F_{net}) without the impact of waves in the Southern Indian Ocean from 2002 to 2021. We also present a time series of F_{net} with waves to evaluate the implications of the CO_2 uptake tread as affected by surface windseas (Figure 10). In each of these diagrams, the scattered points are seasonally averaged values integrated for the entire Southern Indian Ocean, and the lines are independent trends fitted for the corresponding seasons.

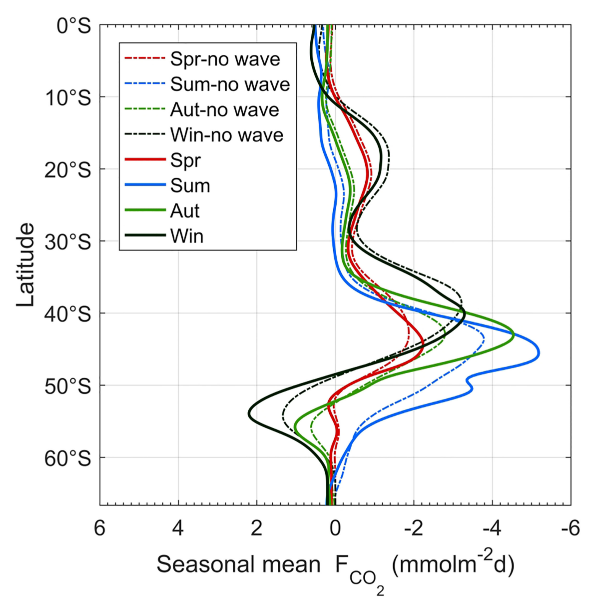

FIGURE 9
Seasonal mean zonal flux (mmol/m^2·d) from 2002 to 2021 in the Southern Indian Ocean. Dashed lines are flux calculated with no waves and solid lines are calculated with waves.

In the last two decades, F_{net} was negative in all four seasons, which means that the Southern Indian Ocean is a perennial carbon sink. Among the different seasons, summer had the largest F_{net}, with an annual mean value without the influence of breaking waves of approximately -0.031 PgC. This was followed by winter, with an annual mean F_{net} of approximately -0.027 PgC, and then by spring and autumn, with annual mean values of -0.022 PgC and -0.021 PgC, respectively. The atmospheric CO_2 absorption capacity of the Southern Indian Ocean gradually strengthened over time. The fitting line between the F_{net} and time clearly shows a decreasing trend. In particular, the correlation shows a relatively smooth trend in the first decade but a much steeper trend in the second decade, which means that the sequestration of atmospheric carbon in the Southern Indian Ocean has become stronger in recent years. Again, summer had the most significant growth rate of F_{net}, with an annual rate of increase of approximately -0.000319 PgC/year with no waves. Under the impact of surface windseas, the annual mean F_{net} shows a clear increasing trend but has a stronger absorbing ability. The largest seasonal improvement is in summer, and the average result over the last 5 years is 32.12%. This indicates that surface wave breaking has a great impact on gas transfer velocity and hence total CO_2 uptake, especially in high wind speed seasons. Even in autumn, surface waves also clearly intensifies the total CO_2 uptake in the Southern Indian Ocean with an improvement of approximately 5.87%. Enter into the latest year, the capacity of CO_2 uptake in the Southern Indian Ocean reach a new peak in 2021. Especially in summer, annual mean value of F_{net} gets to approximately -0.048 PgC with the impact of windseas. These all suggest that a faster process of carbon sequestration is taking place in the Southern Indian Ocean.

4 Discussion and conclusion

Human-induced climate change has led to widespread disruption in nature and is affecting the lives and livelihoods of billions of people (IPCC, 2022a). Air-sea temperature change, sea level rise and extreme weather and climate events have become increasingly prominent due to excess emissions of greenhouse gases. The ocean is an important sink for anthropogenic CO_2 (Siegenthaler and Sarmiento, 1993). Studies have shown that the ocean absorbs more than 25% of the CO_2 emitted by human

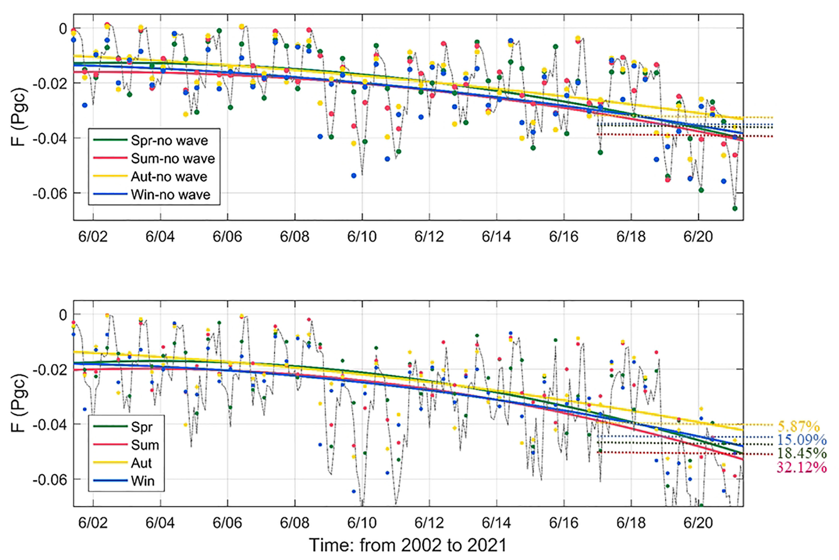

FIGURE 10
Evolution of air-sea net carbon flux, F_{net}(PgC) with waves and no waves in the Southern Indian Ocean. The scattered points are seasonally averaged values integrated for the entire Southern Indian Ocean, and the lines are independent trends fitted for the corresponding seasons.

activities in the atmosphere (Watson et al., 2020) and therefore has a climate-change mitigating effect. The role of the ocean in regulating global climate is significantly affected by the spatiotemporal variation in CO_2 exchange processes at the ocean-atmosphere interface. Although significant importance of the world's carbon cycle and mitigation of anthropogenic climate change, uncertainties remain in quantifying the global marine anthropogenic CO_2 sink as CO_2 uptake by the oceans fails to match emissions from human activities as atmospheric CO_2 levels increase (Khatiwala et al., 2013). At the same time, the ocean will also be negatively affected by climate warming and ocean acidification, further inhibiting its absorption of CO_2 or accelerating its release (Arias-Ortiz et al., 2018; Nakano and Iida, 2018; Aoki et al., 2021).

Surface waves consist of swells and windseas, which are two categories with completely different characteristic features. Previous studies using total waves to quantify the gas transfer velocity may overestimate the impact of waves on the overall CO_2 fluxes. In this study, we highlight the impact of windseas on the process of air-sea CO_2 exchange and address its important role in CO_2 uptake in the Southern Indian Ocean. The main findings of this study are as follows. In the Southern Indian Ocean, previous studies using total waves to modify the air-sea CO_2 transfer rate tended to overestimate the effect of waves. However, we found that windseas, as a main factor influencing gas transfer velocities, contributed only a small fraction of energy to the total waves in almost every region and seasons. Air-sea CO_2 flux showed strong spatiotemporal variation: Regarding seasonality in the Southern Indian Ocean, summer had the strongest CO_2 uptake capacity, with an annual mean flux of approximately −1.8 mmol/m^2·d. The long-term seasonal variations in F_{net} in the Southern Indian Ocean are negative in all seasons, and the fitting correlations of F_{net} with time show a decreasing trend, which means that the sequestration of atmospheric carbon in the Southern Indian Ocean has been strengthening in recent years. This further indicates that the Southern Indian Ocean plays an increasingly important role in influencing global carbon cycling and constraining the global warming process. Meanwhile, the impact of surface waves clearly intensifies the total CO_2 uptake in the Southern Indian Ocean. Under the impact of surface windseas, the annual mean F_{net} shows a clear increasing trend but has a stronger absorbing ability. The largest improvement is in summer, with an average result over the last 5 years of 32.12%. Even in autumn, they have an improvement of approximately 5.87%.

This study presents new findings, but several limitations may still affect the quantitative parts of our results. As lack of direct field measurements of air-sea CO_2 flux, we cannot evaluate the impact of windseas proposed in this study, this is one of a major limitation of this work. Furthermore, we only calculated the CO_2 flux in the open ocean for lack of quantitative synthesis of integrated coastal ocean carbon, which may significantly underestimate the CO_2 uptake process in the entire Southern Indian Ocean. From a global perspective, even though coastal regions account for only 7%-8% of the global ocean area, such regions contribute approximately 28% of the total primary production and help to bury up to 80% of total organic carbon (Dai et al., 2022). Coastal regions are thus one of the most important carbon sinks in the world's oceans and play a crucial role in mitigating global climate change. However, because of the lack of systematic observations and numerical simulations, accounting for these regions in global carbon cycle research remains challenging and has not yet been resolved in this study. In addition, we assumed that the process of ocean absorption of atmospheric CO_2 was solely controlled by certain physical factors. This obviously ignores potential interactions among different factors, such as wind speed, sea surface temperature, and salinity, which may have indirect effects on the CO_2 partial pressure at the surface. Several studies have also provided evidence that changes in SST, SSS, and wind speed can induce variations in the partial pressure of CO_2 *via* physicochemical processes that affect CO_2 exchange (Kashef-Haghighi and Ghoshal, 2013; Sun et al., 2021a; Sun et al., 2021b; Wanninkhof, 1992). We hope that necessary groundwork can be performed to address these problems in future research.

Data availability statement

The original contributions presented in the study are included in the article/supplementary material. Further inquiries can be directed to the corresponding authors.

Author contributions

JY, HZ, and HS conceptualized the research. KZ, JY, and HZ collected the data and contributed expertise to the construction and finalization of the manuscript. HS and KZ conducted the data processing and the main analysis and wrote the manuscript draft. HS and KZ share first authorship. All authors contributed to the article and approved the submitted version.

Funding

This research was financially supported by the National Natural Science Foundation of China (41976017, 42206014 and U20A2099), the Hainan Provincial Joint Project of Sanya Yazhou Bay Science and Technology City (220LH061) and Hainan Provincial Key Research and Development Projects (ZDYF2022SHFZ018).

Acknowledgments

AMSR data are produced by Remote Sensing Systems and were sponsored by the NASA AMSR-E Science Team and the NASA Earth Science MEaSUREs Program. Data are available at www.remss.com. NCEP Global Ocean Data Assimilation System (GODAS) data are provided by NOAA PSL, Boulder, Colorado, USA, from their website at https://psl.noaa.gov. The air-sea CO_2 partial pressure products are produced by NOAA National Centers for Environmental Information (DOI: https://doi.org/10.7289/

V5Z899N6). The altimeter data in this study was obtained from Australian Ocean Data Network.

Conflict of interest

The authors declare that the research was conducted in the absence of any commercial or financial relationships that could be construed as a potential conflict of interest.

Publisher's note

References

Anoop, T. R., Shanas, P. R., Aboobacker, V. M., Kumar, V. S., Nair, L. S., Prasad, R., et al. (2020). On the generation and propagation of makran swells in the Arabian Sea. *Int. J. Climatol.* 40 (1), 585–593. doi: 10.1002/joc.6192

Aoki, L. R., McGlathery, K. J., Wiberg, P. L., Oreska, M. P., Berger, A. C., Berg, P., et al. (2021). Seagrass recovery following marine heat wave influences sediment carbon stocks. *Front. Mar. Sci.* 7. doi: 10.3389/fmars.2020.576784

Arias-Ortiz, A., Serrano, O., Masqué, P., Lavery, P. S., Mueller, U., Kendrick, G. A., et al. (2018). A marine heatwave drives massive losses from the world's largest seagrass carbon stocks. *Nat. Clim. Change.* 8 (4), 338–344. doi: 10.1038/s41558-018-0096-y

Bakker, D. C. E., Pfeil, B., Landa, C. S., Metzl, N., O'Brien, K. M., Olsen, A., et al. (2016). A multi-decade record of high-quality fCO_2 data in version 3 of the surface ocean CO_2 atlas (SOCAT). *Earth. Syst. Sci. Data.* 8, 383–413. doi: 10.5194/essd-8-383-2016

Bates, N. R., Pequignet, A. C., and Sabine, C. L. (2006). Ocean carbon cycling in the Indian ocean: 1. spatiotemporal variability of inorganic carbon and air-sea CO_2 gas exchange. *Global Biogeochem. Cy.* 20 (3), GB3020. doi: 10.1029/2005GB002491

Behringer, D. W., Ji, M., and Leetmaa, A. (1998). An improved coupled model for ENSO prediction and implications for ocean initialization. part I: The ocean data assimilation system. *Mon. Wea. Rev.* 126 (4), 1013–1021. doi: 10.1175/1520-0493(1998)126<1022:AICMFE>2.0.CO;2

Brumer, S. E., Zappa, C. J., Blomquist, B. W., Fairall, C. W., Cifuentes-Lorenzen, A., Edson, J. B., et al. (2017). Wave-related reynolds number parameterizations of CO2 and DMS transfer velocities. *Geophys. Res. Lett.* 44 (19), 9865–9875. doi: 10.1002/2017GL074979

Dai, M., Su, J., Zhao, Y., Hofmann, E. E., Cao, Z., Cai, W. J., et al. (2022). Carbon fluxes in the coastal ocean: Synthesis, boundary processes and future trends. *Annu. Rev. Earth Planet. Sci.* 50, 593–626. doi: 10.1146/annurev-earth-032320-090746

Deacon, E. L. (1977). Gas transfer to and across an air-water interface. *Tellus* 29 (4), 363–374. doi: 10.3402/tellusa.v29i4.11368

Deacon, E. L. (1981). Sea-Air gas transfer: The wind speed dependence. *Boundary. Layer. Meteorol.* 21 (1), 31–37. doi: 10.1007/BF00119365

Deike, L., and Melville, W. K. (2018). Gas transfer by breaking waves. *Geophys. Res. Lett.* 45 (19), 10–482. doi: 10.1029/2018GL078758

DeVries, T. (2014). The oceanic anthropogenic CO_2 sink: Storage, air-sea fluxes, and transports over the industrial era. *Global Biogeochem. Cy.* 28 (7), 631–647. doi: 10.1002/2013GB004739

Edson, J. B., Fairall, C. W., Bariteau, L., Zappa, C. J., Cifuentes-Lorenzen, A., McGillis, W. R., et al. (2011). Direct covariance measurementof CO_2 gas transfer velocity during the 2008 southern ocean gas exchange experiment: Wind speed dependency. *J. Geophys. Res. Oceans.* 116 (C4), C00F10. doi: 10.1029/2011JC007022

Ethamony, P. V., Rashmi, R., Samiksha, S. V., and Aboobacker, V. M. (2013). Recent studies on wind seas and swells in the Indian ocean: A review. *Int. J. Ocean. Climate Systems.* 4 (1), 63–73. doi: 10.1260/1759-3131.4.1.63

Feely, R. A., Sabine, C. L., Takahashi, T., and Wanninkhof, R. (2001). Uptake and storage of carbon dioxide in the ocean: The global CO_2 survey. *Oceanography* 14 (4), 18–32. doi: 10.5670/oceanog.2001.03

Friedlingstein, P., O'sullivan, M., Jones, M. W., Andrew, R. M., Hauck, J., Olsen, A., et al. (2020). Global carbon budget 2020. *Earth. Syst. Sci. Data.* 12 (4), 3269–3340. doi: 10.5194/essd-12-3269-2020

Frölicher, T. L., Sarmiento, J. L., Paynter, D. J., Dunne, J. P., Krasting, J. P., and Winton, M. (2015). Dominance of the southern ocean in anthropogenic carbon and heat uptake in CMIP5 models. *J. Clim.* 28 (2), 862–886. doi: 10.1175/JCLI-D-14-00117.1

Gruber, N., Landschützer, P., and Lovenduski, N. S. (2019). The variable southern ocean carbon sink. *Ann. Rev. Mar. Sci.* 11, 159–186. doi: 10.1146/annurev-marine-121916-063407

Gu, Y., Katul, G. G., and Cassar, N. (2021). The intensifying role of high wind speeds on air-sea carbon dioxide exchange. *Geophys. Res. Lett.* 48 (5), e, 2020GL090713. doi: 10.1029/2020GL090713

Gu, Y., Katul, G. G., and Cassar, N. (2020). Mesoscale temporal wind variability biases global air–sea gas transfer velocity of CO2 and other slightly soluble gases. *Remote Sensing* 13 (7), 1328. doi: 10.3390/rs13071328

Hanson, J. L., and Jensen, R. E. (2004). "Wave system diagnostics for numerical wave models," *Proceedings of the 8th International Work-shop on Wave Hindcasting and Forecasting.* (Oahu, Hawaii), 231–238.

Hanson, J. L., Tracy, B., Tolman, H. L., and Scott, D. (2006). "Pacific hindcast performance evaluation of three numerical wave models," in *9th international workshop on wave hindcasting and forecasting*(Victoria, BC, Canada), 1324–1338.

Hasse, L., and Liss, P. S. (1980). Gas exchange across the air-sea interface. *Tellus* 32 (5), 470–481. doi: 10.3402/tellusa.v32i5.10602

IPCC (2022a). *Climate change 2022: Impacts, adaptation, and vulnerability. contribution of working group II to the sixth assessment report of the intergovernmental panel on climate change.* Eds. H.-O. Pörtner, D. C. Roberts, M. Tignor, E. S. Poloczanska, K. Mintenbeck, A. Alegría, M. Craig, S. Langsdorf, S. Löschke, V. Möller, A. Okem and B. Rama (Cambridge, UK and New York, NY, USA: Cambridge University Press), 3056. doi: 10.1017/9781009325844

IPCC (2022b). *Climate change 2022: Mitigation of climate change. contribution of working group III to the sixth assessment report of the intergovernmental panel on climate change.* Eds. P. R. Shukla, J. Skea, R. Slade, A. Al Khourdajie, R. van Diemen, D. McCollum, M. Pathak, S. Some, P. Vyas, R. Fradera, M. Belkacemi, A. Hasija, G. Lisboa, S. Luz and J. Malley (Cambridge, UK and New York, NY, USA: Cambridge University Press). doi: 10.1017/9781009157926

Jabaud-Jan, A., Metzl, N., Brunet, C., Poisson, A., and Schauer, B. (2004). Interannual variability of the carbon dioxide system in the southern Indian ocean (20°S–60°S): The impact of a warm anomaly in austral summer 1998. *Global Biogeochem. Cy.* 18 (1), GB1042. doi: 10.1029/2002GB002017

Jiang, H., and Chen, G. (2013). A global view on the swell and wind sea climate by the Jason-1 mission: A revisit. *J. Atmospheric. Oceanic. Technol.* 30 (8), 1833–1841. doi: 10.1175/JTECH-D-12-00180.1

Joos, F., and Spahni, R. (2008). Rates of change in natural and anthropogenic radiative forcing over the past 20,000 years. *Proc. Natl. Acad. Sci.* 105 (5), 1425–1430. doi: 10.1073/pnas.0707386105

Kashef-Haghighi, S., and Ghoshal, S. (2013). Physico-chemical processes limiting CO2 uptake in concrete during accelerated carbonation curing. *Ind. Eng. Chem. Res.* 52 (16), 5529–5537. doi: 10.1021/ie303275e

Keeling, R. F. (1993). On the role of large bubbles in air-sea gas exchange and supersaturation in the ocean. *J. Mar. Res.* 51 (2), 237–271. doi: 10.1357/0022240933223800

Khatiwala, S., Tanhua, T., Mikaloff Fletcher, S., Gerber, M., Doney, S. C., Graven, H. D., et al. (2013). Global ocean storage of anthropogenic carbon. *Biogeosciences* 10 (4), 2169–2191. doi: 10.5194/bg-10-2169-2013

Komori, S., and Misumi, R. (2002). The effects of bubbles on mass transfer across the breaking air-water interface. *Washington. DC. Am. Geophys. Union. Geophys. Monograph. Series.* 127, 285–290. doi: 10.1029/GM127p0285

Lacis, A. A., Schmidt, G. A., Rind, D., and Ruedy, R. A. (2010). Atmospheric CO_2: Principal control knob governing earth's temperature. *Science* 330 (6002), 356–359. doi: 10.1126/science.1190653

Landschützer, P., Gruber, N., and Bakker, D. C. (2020). *Data from: An observation-based global monthly gridded sea surface pCO2 product from 1982 onward and its monthly climatology (NCEI accession 0160558). version 5.5* (NOAA National Centers for Environmental Information). doi: 10.7289/V5Z899N6

Lekshmi, K., Bharti, R., and Mahanta, C. (2021). Dynamics of air-sea carbon dioxide fluxes and their trends in the global context. *Curr. Sci.* 121 (5), 626–640. doi: 10.18520/cs/v121/i5/626-640

Lenain, L., and Melville, W. K. (2017). Measurements of the directional spectrum across the equilibrium saturation ranges of wind-generated surface waves. *J. Phys. Oceanogr.* 47 (8), 2123–2138. doi: 10.1175/JPO-D-17-0017.1

Levitus, S., Antonov, J. I., Boyer, T. P., and Stephens, C. (2000). Warming of the world ocean. *Science* 287 (5461), 2225–2229. doi: 10.1126/science.287.5461.2225

Li, S., Babanin, A. V., Qiao, F., Dai, D., Jiang, S., and Guan, C. (2021). Laboratory experiments on CO_2 gas exchange with wave breaking. *J. Phys. Oceanogr.* 51 (10), 3105–3116. doi: 10.1175/JPO-D-20-0272.1

Liang, J.-H., D'Asaro, E. A., McNeil, C. L., Fan, Y., Harcourt, R. R., Emerson, S. R., et al. (2020). Suppression of CO_2 outgassing by gas bubbles under a hurricane. *Geophys. Res. Lett.* 47, e2020GL090249. doi: 10.1029/2020GL090249

Liang, J. H., Deutsch, C., McWilliams, J. C., Baschek, B., Sullivan, P. P., and Chiba, D. (2013). Parameterizing bubble-mediated air-sea gas exchange and its effect on ocean ventilation. *Global Biogeochem. Cy.* 27 (3), 894–905. doi: 10.1002/gbc.20080

Liu, J. F., Jiang, W., and Yu, M. G. (2002). An analysis on annual variation of monthly mean sea wave fields in north pacific ocean. *J. Trop. Oceanography.* 21 (3), 364–369.

Louanchi, F., Metzl, N., and Poisson, A. (1996). Modelling the monthly sea surface fCO_2 fields in the Indian ocean. *Mar. Chem.* 55 (3-4), 265–279. doi: 10.1016/S0304-4203(96)00066-7

McGillis, W. R., Edson, J. B., Ware, J. D., Dacey, J. W., Hare, J. E., Fairall, C. W., et al. (2001). Carbon dioxide flux techniques performed during GasEx-98. *Mar. Chem.* 75 (4), 267–280. doi: 10.1016/S0304-4203(01)00042-1

Metzl, N., Poisson, A., Louanchi, F., Brunet, C., Schauer, B., and Bres, B. (1995). Spatio-temporal distributions of air-sea fluxes of CO_2 in the Indian and Antarctic oceans: A first step. *Tellus. B.* 47 (1-2), 56–69. doi: 10.1034/j.1600-0889.47.issue1.7.x

Monteiro, T., Kerr, R., and Machado, E. D. C. (2020). Seasonal variability of net sea-air CO_2 fluxes in a coastal region of the northern Antarctic peninsula. *Sci. Rep.* 10 (1), 1–15. doi: 10.1038/s41598-020-71814-0

Nakano, T., and Iida, Y. (2018). Ocean acidification and carbon dioxide uptake in the global ocean. *PICES. Press* 26 (1), 34–36.

Qian, C., Jiang, H., Wang, X., and Chen, G. (2020). Climatology of wind-seas and swells in the China seas from wave hindcast. *J. Ocean. Univ. China.* 19, 90–100. doi: 10.1007/s11802-020-3924-4

Reichl, B. G., and Deike, L. (2020). Contribution of sea-state dependent bubbles to air-sea carbon dioxide fluxes. *Geophys. Res. Lett.* 47 (9), e2020GL087267. doi: 10.1029/2020GL087267

Ribal, A., and Young, I. R. (2019). 33 years of globally calibrated wave height and wind speed data based on altimeter observations. *Sci. Data.* 6 (1), 1–15. doi: 10.1038/s41597-019-0083-9

Roobaert, A., Laruelle, G. G., Landschützer, P., Gruber, N., Chou, L., and Regnier, P. (2019). The spatiotemporal dynamics of the sources and sinks of CO_2 in the global coastal ocean. *Global Biogeochem. Cy.* 33 (12), 1693–1714. doi: 10.1029/2019GB006239

Sabine, C. L., Feely, R. A., Gruber, N., Key, R. M., Lee, K., Bullister, J. L., et al. (2004). The oceanic sink for anthropogenic CO_2. *Science* 305 (5682), 367–371. doi: 10.1126/science.1097403

Sarma, V. V. S. S., Lenton, A., Law, R. M., Metzl, N., Patra, P. K., Doney, S., et al. (2013). Sea-Air CO_2 fluxes in the Indian ocean between 1990 and 2009. *Biogeosciences* 10 (11), 7035–7052. doi: 10.5194/bg-10-7035-2013

Schmidt, G. A., Ruedy, R. A., Miller, R. L., and Lacis, A. A. (2010). Attribution of the present-day total greenhouse effect. *J. Geophys. Res. Atmos.* 115 (D20), D20106. doi: 10.1029/2010JD014287

Semedo, A., Sušelj, K., Rutgersson, A., and Sterl, A. (2011). A global view on the wind sea and swell climate and variability from ERA-40. *J. Clim.* 24 (5), 1461–1479. doi: 10.1175/2010JCLI3718.1

Siegenthaler, U., and Sarmiento, J. L. (1993). Atmospheric carbon dioxide and the ocean. *Nature* 365 (6442), 119–125. doi: 10.1038/365119a0

Sun, Z., Shao, W., Wang, W., Zhou, W., Yu, W., and Shen, W. (2021a). Analysis of wave-induced stokes transport effects on sea surface temperature simulations in the Western pacific ocean. *J. Mar. Sci. Engineering.* 9 (8), 834. doi: 10.3390/jmse9080834

Sun, Z., Shao, W., Yu, W., and Li, J. (2021b). A study of wave-induced effects on sea surface temperature simulations during typhoon events. *J. Mar. Sci. Engineering.* 9 (6), 622. doi: 10.3390/jmse9060622

Takahashi, T., Sutherland, S. C., Sweeney, C., Poisson, A., Metzl, N., Tilbrook, B., et al. (2002). Global sea-air CO_2 flux based on climatological surface ocean pCO_2, and seasonal biological and temperature effects. *Deep. Sea. Res. 2 Top. Stud. Oceanogr.* 49 (9-10), 1601–1622. doi: 10.1016/S0967-0645(02)00003-6

Tao, A., Yan, J., Pei, Y., Zheng, J., and Mori, N. (2017). Swells of the East China sea. *J. Ocean. Univ. China.* 16, 674–682. doi: 10.1007/s11802-017-3406-5

Toba, Y. (1988). Similarity laws of the wind wave and the coupling process of the air and water turbulent boundary layers. *Fluid. Dynamics. Res.* 2 (4), 263. doi: 10.1016/0169-5983(88)90005-6

Toba, Y., and Koga, M. (1986). "A parameter describing overall conditions of wave breaking, whitecapping, sea-spray production and wind stress," in *Oceanic whitecaps* (Dordrecht: Springer), 37–47.

Valsala, V., Maksyutov, S., and Murtugudde, R. (2012). A window for carbon uptake in the southern subtropical Indian ocean. *Geophys. Res. Lett.* 39 (17), L17605. doi: 10.1029/2012GL052857

Vieira, V. M. N. C., Mateus, M., Canelas, R., and Leitão, F. (2020). The FuGas 2.5 updated for the effects of surface turbulence on the transfer velocity of gases at the atmosphere–ocean interface. *J. Mar. Sci. Eng.* 8, 435.

Vincent, L., and Soille, P. (1991). Watersheds in digital spaces: an efficient algorithm based on immersion simulations. *IEEE Trans. Pattern Anal. Mach. Intell.* 13 (06), 583–598. doi: 10.1109/34.87344

Wang, W., and Huang, R. X. (2004). Wind energy input to the surface waves. *J. Phys. Oceanogr.* 34 (5), 1276–1280. doi: 10.1175/1520-0485(2004)034<1276:WEITTS>2.0.CO;2

Wanninkhof, R. (1992). Relationship between wind speed and gas exchange over the ocean. *J. Geophys. Res. Oceans.* 97 (C5), 7373–7382. doi: 10.1029/92JC00188

Wanninkhof, R. (2014). Relationship between wind speed and gas exchange over the ocean revisited. *Limnol. Oceanogr. Methods* 12 (6), 351–362. doi: 10.4319/lom.2014.12.351

Wanninkhof, R., and Triñanes, J. (2017). The impact of changing wind speeds on gas transfer and its effect on global air-sea CO_2 fluxes. *Global Biogeochem. Cycles.* 31 (6), 961–974. doi: 10.1002/2016GB005592

Watson, A. J., Schuster, U., Shutler, J. D., Holding, T., Ashton, I. G., Landschützer, P., et al. (2020). Revised estimates of ocean-atmosphere CO_2 flux are consistent with ocean carbon inventory. *Nat. Commun.* 11 (1), 1–6. doi: 10.1038/s41467-020-18203-3

Weiss, R. (1974). Carbon dioxide in water and seawater: the solubility of a non-ideal gas. *Mar. Chem.* 2 (3), 203–215. doi: 10.1016/0304-4203(74)90015-2

Willeit, M., Ganopolski, A., Calov, R., and Brovkin, V. (2019). Mid-pleistocene transition in glacial cycles explained by declining CO_2 and regolith removal. *Sci. Adv.* 5 (4), eaav7337. doi: 10.1126/sciadv.aav7337

Woolf, D. K. (1993). Bubbles and the air-sea transfer velocity of gases. *Atmosphere-Ocean* 31 (4), 517–540. doi: 10.1029/2018GB006041

Xu, S., Chen, L., Chen, H., Li, J., Lin, W., and Qi, D. (2016). Sea-Air CO_2 fluxes in the southern ocean for the late spring and early summer in 2009. *Remote Sens. Environ.* 175, 158–166. doi: 10.1016/j.rse.2015.12.049

Zappa, C. J., McGillis, W. R., Raymond, P. A., Edson, J. B., Hintsa, E. J., Zemmelink, H. J., et al. (2007). Environmental turbulent mixing controls on air-water gas exchange in marine and aquatic systems. *Geophys. Res. Lett.* 34 (10), L10601. doi: 10.1029/2006GL028790

Zhang, M., Marandino, C. A., Chen, L., Sun, H., Gao, Z., Park, K., et al. (2017). Characteristics of the surface water DMS and pCO2 distributions and their relationships in the southern ocean, southeast Indian ocean, and northwest pacific ocean. *Global Biogeochem. Cy.* 31 (8), 1318–1331. doi: 10.1002/2017GB005637

Zhang, J., Wang, W., and Guan, C. (2011). Analysis of the global swell distributions using ECMWF re-analyses wind wave data. *J. Ocean. Univ. China.* 10, 325–330. doi: 10.1007/s11802-011-1859-5

Zhao, D., Toba, Y., Suzuki, Y., and Komori, S. (2003). Effect of wind waves on air'sea gas exchange: Proposal of an overall CO_2 transfer velocity formula as a function of breaking-wave parameter. *Tellus. B.* 55 (2), 478–487. doi: 10.1034/j.1600-0889.2003.00055.x

Zheng, Z., Luo, X., Wei, H., Zhao, W., and Qi, D. (2021). Analysis of the seasonal and interannual variations of air-sea CO_2 flux in the chukchi Sea using a coupled ocean-sea ice-biogeochemical model. *J. Geophys. Res. Oceans.* 126 (8), e2021JC017550. doi: 10.1029/2021JC017550

Zheng, K., Sun, J., Guan, C., and Shao, W. (2016). Analysis of the global swell and wind sea energy distribution using WAVEWATCH III. *Adv. Meteorol.* 10, 1–9. doi: 10.1155/2016/8419580